ON THE BLOCH DECOMPOSITION BASED SPECTRAL METHOD FOR WAVE PROPAGATION IN PERIODIC MEDIA

ZHONGYI HUANG, SHI JIN, PETER A. MARKOWICH, AND CHRISTOF SPARBER

Abstract. We extend the Bloch-decomposition based time-splitting spectral method introduced in an earlier paper [13] to the case of (non-)linear Klein-Gordon equations. This provides us with an unconditionally stable numerical method which achieves spectral convergence in space, even in the case where the periodic coefficients are highly oscillatory and/or discontinuous. A comparison to a traditional pseudo-spectral method and to a finite difference/volume scheme shows the superiority of our method. We further estimate the stability of our scheme in the presence of random perturbations and give numerical evidence for the well-known phenomenon of Anderson's localization.

version: February 15, 2008

1. Introduction

In this paper we consider the propagation of (nonlinear) *high frequency* waves in a one-dimensional medium with a *periodic microstructure*. Such problems arise, e.g., in the study of composite materials, photonic crystals, optic lattices [5]. For instance, the propagation of linearly polarized light in a fiber Bragg grating with intensity dependent refraction-index χ, i.e. a so-called Kerr medium, can be modelled by the nonlinear wave equation, cf. [6, 24],

$$\frac{\partial^2 E}{\partial t^2} = \chi_{\rm lin}(x)\frac{\partial^2 E}{\partial x^2} - \chi_{\rm lin}(x)E - \chi_{\rm nl}(x)E^3. \tag{1.1}$$

Here E is the remaining (single) component of the electric field, $\chi_{\rm lin}$ denotes the square of the linear index of refraction and $\chi_{\rm nl}$ the corresponding nonlinear Kerr-susceptibility. Both coefficients are *spatially periodic* functions.

In the following we shall be interested in the case where the typical wavelength is comparable to the period of the medium, and both of which are assumed to be small on the length-scale of the considered physical domain, i.e. on the scale observation. This consequently leads us to a problem invoking *two-scales* where from now on we shall denote by $0 < \varepsilon \ll 1$ the small dimensionless parameter describing the microscopic/macroscopic scale ratio. In this paper we shall study of the following class of (one-dimensional)

2000 *Mathematics Subject Classification.* 65M70, 74Q10, 35B27, 81Q20.

Key words and phrases. Klein-Gordon equation, Wave propagation, Bloch decomposition, time-splitting spectral method, periodic structure, Anderson localization.

This work was partially supported the Austrian-Chinese Technical-Scientific Cooperation Agreement, the NSF grant No. DMS-0608720, the NSFC Projects 10301017, 10676017, and 10228101, and the National Basic Research Program of China, grant no. 2005CB321701. S. Jin was also supported by a "Van Vleck Distinguished Research Prize" from the University of Wisconsin-Madison. C. Sparber. has been supported by the "APART grant" of the Austrian Academy of Science. P. Markowich acknowledges support from the Royal Society through his "Wolfson Research Merit Award".

Klein-Gordon type equations

$$\begin{cases} \dfrac{\partial^2 u}{\partial t^2} = \dfrac{\partial}{\partial x}\left(a_\Gamma\left(\dfrac{x}{\varepsilon}\right)\dfrac{\partial u}{\partial x}\right) - \dfrac{1}{\varepsilon^2} W_\Gamma\left(\dfrac{x}{\varepsilon}\right) u + f(x), \quad x \in \mathbb{R},\, t > 0, \\ u\big|_{t=0} = u_0(x), \quad \dfrac{\partial u}{\partial t}\big|_{t=0} = v_0(x), \end{cases} \tag{1.2}$$

with given initial data $u_0(x), v_0(x) \in \mathbb{R}$ and $f(x) \in \mathbb{R}$ describing some slowly varying source term. A nonlinear version of this model, similar to equation (1.1), will also be considered later on (see Example 3.3). The highly oscillatory coefficients $a_\Gamma(y), W_\Gamma(y) \in \mathbb{R}$ are assumed to be *periodic* with respect to some *regular lattice* $\Gamma \simeq \mathbb{Z}$. Equation (1.2) henceforth describes the propagation of waves on macroscopic length- and time-scales.

Concerning the numerical simulation of such problems, we note that in [8] Fogarty and LeVeque provided high-resolution finite-volume methods for acoustic waves propagation in periodic and random media. The reader can find more related works in [17, 19]. Indeed, the main computational challenge in the simulations of equations like (1.2), stems from the fact that the computational grid size must be small enough to capture the microscopic details of the medium, or, equivalently, the shortest wavelength. Furthermore, having in mind the CFL conditions in traditional finite-difference or finite-volume schemes, also the time-steps have to be chosen small enough, i.e. $\mathcal{O}(\varepsilon)$. Therefore, the overall computational costs become prohibitively expensive.

One possibility to circumvent such problems is to entirely rely on *homogenized equations* which approximate (1.2) in the limit $\varepsilon \to 0$, cf. [1, 5, 23, 24] for the derivation of such models. Numerical studies in this spirit can be found in [22] where the authors derive an effective dispersive model describing wave propagation in a periodic medium. Similarly, Kevorkian and Bosley [16] considered hyperbolic conservation laws with rapidly varying, spatially periodic fluctuations by multiple asymptotic analysis. Numerical approaches on the related problem of linear Schrödinger equation with a periodic potential were studied in [11, 12]. However, by passing to an effective (homogenized) equation, one usually looses all details of the underlying microscopic dynamics. In particular this prohibits one to simulate and compare the behavior for different choices for $\varepsilon > 0$. It is therefore highly desirable to design a numerical method that, for any given wavelength, i.e. for any given choice of ε, allows for rather large mesh-size and/or time-steps. We have done so in our earlier works [13, 14], where we considered (nonlinear) Schrödinger equations with periodic potentials. There, we developed a Bloch-decomposition based spectral method for which has been demonstrated to be superior to traditional Fourier spectral methods. The main advantages of our new method include: Spectral accuracy in space even in the case of discontinuous periodic coefficients and the possibility of choosing large time steps, i.e. of order $\mathcal{O}(1)$, even for small wave length. In the present work, we shall extend our Bloch-decomposition based time-splitting scheme to evolutionary problems of the above given Klein-Gordon type (including nonlinearities).

We outline the contents of the paper here. We first give a short review on the analytical background of the Bloch decomposition in Section 2 and we consequently show how to apply it numerically to equations of the form (1.2). Next, we compare our method with the more traditional pseudo-spectral method and with a finite-volume scheme in Section 3. In particular, we also include a (weakly) nonlinear case there. In Section 4 we shall also take into account *random coefficients* $a_\Gamma(\omega, y)$ to test the stability of our scheme with respect to random perturbations. Finally, we shall study the wave propagation in *random media* and give numerical evidence for the emergence of so-called *Anderson's localization*.

2. Description of the Bloch-decomposition based numerical method

In this section we will briefly recapitulate the numerical method developed in [13] and discuss its extension to the Klein-Gordon equation (1.2). For the convenience of the reader we shall first recall some basic definitions and important facts which are used when dealing with periodic operators.

2.1. **Review of the Bloch decomposition.**

For definiteness, we shall assume from now on that

$$a_\Gamma(y+2\pi) = a_\Gamma(y), \quad W_\Gamma(y+2\pi) = W_\Gamma(y), \quad \forall\, y \in \mathbb{R}, \tag{2.1}$$

i.e. $\Gamma = 2\pi\mathbb{Z}$. Here, and in all what follows we shall always denote $y = x/\varepsilon$. Furthermore, we assume that

$$a_\Gamma(y) \geq a_0 > 0, \quad \forall\, y \in [0, 2\pi]. \tag{2.2}$$

in order to ensure ellipticity in the eigenvalue-problem (2.3) below. For $\Gamma = 2\pi\mathbb{Z}$, it holds [3]:

- The fundamental domain of our lattice is $\mathcal{C} = (0, 2\pi)$.
- The *dual lattice* Γ^* is simply given by $\Gamma^* = \mathbb{Z}$.
- The fundamental domain of the dual lattice $\mathcal{B} = \mathcal{C}^*$, i.e. the (first) *Brillouin zone*, is $\mathcal{B} = \left(-\frac{1}{2}, \frac{1}{2}\right)$.

Next, consider the eigenvalue problem,

$$\left(-\frac{\partial}{\partial_y}\Big(a_\Gamma(y)\frac{\partial}{\partial_y}\Big) + W_\Gamma(y)\right)\varphi_m(y,k) = \lambda_m(k)\varphi_m(y,k), \tag{2.3}$$

subject to the quasi-periodic boundary condition

$$\varphi_m(y+2\pi,k) = \mathrm{e}^{\mathrm{i}2\pi k y}\varphi_m(y,k), \quad \forall\, k \in \mathcal{B}. \tag{2.4}$$

Under the assumption (2.1), (2.2), it is well known (see [28, 5]), that the problem (2.3) admits has a countable family of *real eigenvalues* $\lambda_m(k) \equiv E_m^2(k) \geq 0$, which can be ordered according to

$$E_1^2(k) \leq E_2^2(k) \leq \cdots \leq E_m^2(k) \leq \cdots, \ m \in \mathbb{N},$$

taking into account the respective multiplicity. The set $\{E_m^2(k) \,|\, k \in \mathcal{B}\} \subset \mathbb{R}$ is called the m-th *energy band* of the operator H. (In the following the index $m \in \mathbb{N}$ will *always* denote the *band index*.) Correspondingly, there exists a complete set of *eigenfunctions* $\varphi_m(y,k)$, $m \in \mathbb{N}$, which, for each fixed $k \in \overline{\mathcal{B}}$, provide an orthonormal basis in $L^2(\mathcal{C})$.

By solving the eigenvalue problem (2.3), the Bloch decomposition allows to decompose the Hilbert space $\mathcal{H} = L^2(\mathbb{R})$ into a direct sum of orthogonal *band spaces* [18, 20, 28], i.e.

$$L^2(\mathbb{R}) = \bigoplus_{m=1}^{\infty} \mathcal{H}_m, \quad \mathcal{H}_m := \left\{ \psi_m(y) = \int_{\mathcal{B}} \Psi(k)\, \varphi_m(y,k)\, \mathrm{d}k, \ \Psi \in L^2(\mathcal{B}) \right\}. \tag{2.5}$$

This consequently allows us to write

$$\forall\, \psi \in L^2(\mathbb{R}): \quad \psi(y) = \sum_{m\in\mathbb{N}} \psi_m(y), \quad \psi_m \in \mathcal{H}_m. \tag{2.6}$$

The corresponding projection of ψ onto the m-th band space is given by [18]

$$\psi_m(y) \equiv (\mathbb{P}_m\psi)(y) = \int_{\mathcal{B}} C_m(k)\varphi_m(y,k)\, \mathrm{d}k, \tag{2.7}$$

where we denote by

$$C_m(k) := \int_{\mathbb{R}} \psi(\zeta)\overline{\varphi}_m(\zeta,k)\, \mathrm{d}\zeta, \tag{2.8}$$

the coefficient of the Bloch-decomposition.

2.2. **The Bloch decomposition based split-step algorithm.** In [13] we introduced a numerical method for periodic Schrödinger equations, which is based on the Bloch decomposition described above. In order to make the present paper self-contained, we shall recall here the most important steps of our algorithm and show how to apply it to equations of the form (1.2). For more details, discussion etc. we refer to [13, 14].

As a necessary preprocessing, we first need to calculate the energy bands $E_m(k)$ as well as the eigenfunction $\varphi_m(y,k)$ from (2.3). In $d=1$ dimension this is rather easy as has been described in [13]. We shall therefore not go into details here and only remark that the numerical cost for this preprocessing does not depend on the spatial grid chosen to simulate the considered evolutionary problem. These costs are therefore almost negligible when compared to the costs spent in the evolutionary algorithms below.

We consider the equation (1.2) on a bounded domain $\mathcal{D}=[0,2\pi]$ supplemented by *periodic boundary conditions*. This represents an approximation of our (one-dimensional) whole-space problem, as long as the observed solution $u(t,x)$ does not touch the boundaries $x=0,2\pi$. Let $L\in\mathbb{N}$ be the number of lattice cells within this computational domain $\mathcal{D}$, and further let $R\in\mathbb{N}$ be the number of grid points in each lattice cell. This consequently yields the following discretization

$$\begin{cases} k_\ell = -\dfrac{1}{2}+\dfrac{\ell-1}{L}, & \text{where } \ell=\{1,\cdots,L\}\subset\mathbb{N},\\ y_r = \dfrac{2\pi(r-1)}{R}, & \text{where } r=\{1,\cdots,R\}\subset\mathbb{N}. \end{cases} \tag{2.9}$$

Thus, for any time-step t_n, we evaluate $u(t_n,\cdot)$, the solution of (1.2), at the grid points

$$x_{\ell,r} = \varepsilon\big(2\pi(\ell-1)+y_r\big). \tag{2.10}$$

Let us introduce the following unitary transformation of $\psi\in L^2(\mathbb{R})$

$$(\mathcal{T}\psi)(y,k)\equiv\widetilde{\psi}(y,k) := \sum_{\gamma\in\mathbb{Z}}\psi(\varepsilon(y+2\pi\gamma))\,\mathrm{e}^{-\mathrm{i}2\pi k\gamma},\quad y\in\mathcal{C},\ k\in\mathcal{B}, \tag{2.11}$$

such that $\widetilde{\psi}(y+2\pi,k)=\mathrm{e}^{2\mathrm{i}\pi k}\widetilde{\psi}(y,k)$ and $\widetilde{\psi}(y,k+1)=\widetilde{\psi}(y,k)$. In other words $\widetilde{\psi}(y,k)$ admits the same periodicity properties w.r.t. k and y as the Bloch eigenfunction $\varphi_m(y,k)$. Thus we can decompose $\widetilde{\psi}(y,k)$ as a linear combination of such states $\varphi_m(y,k)$. The transform $\mathcal{T}$ allows to circumvent the implementation of a numerical Bloch transformation and to solely rely on the classical Fast Fourier transform (FFT). Note that the following inversion formula for $\mathcal{T}$ holds

$$\psi(\varepsilon(y+2\pi\gamma)) = \int_{\mathcal{B}}\widetilde{\psi}(y,k)\,\mathrm{e}^{\mathrm{i}2\pi k\gamma}\mathrm{d}k. \tag{2.12}$$

Moreover one easily sees that the Bloch coefficient, defined in (2.8), can be equivalently be written as

$$C_m(k) = \int_{\mathcal{C}}\widetilde{\psi}(y,k)\overline{\varphi}_m(y,k)\,\mathrm{d}y. \tag{2.13}$$

We are now in position to set up the time-splitting algorithm. We solve (1.2) in two steps.

Step 1. First, we solve the system of equations

$$\begin{cases} \dfrac{\partial u}{\partial t} = v, & u\big|_{t=0}=u_0(x),\\ \dfrac{\partial v}{\partial t} = \dfrac{\partial}{\partial x}\left(a_\Gamma\left(\dfrac{x}{\varepsilon}\right)\dfrac{\partial u}{\partial x}\right)-\dfrac{1}{\varepsilon^2}W_\Gamma\left(\dfrac{x}{\varepsilon}\right)u, & v\big|_{t=0}=v_0(x), \end{cases} \tag{2.14}$$

on a fixed time-interval $\triangle t$. To do so we consider for each fixed $t \in \mathbb{R}$, the corresponding transformed solution $(\mathcal{T}u(t,\cdot)) \equiv \widetilde{u}(t,y,k)$ and $(\mathcal{T}v(t,\cdot)) \equiv \widetilde{v}(t,y,k)$, where $\mathcal{T}$ is defined in (2.11). We consequently decompose $\widetilde{u}(t,y,k)$ according to

$$\widetilde{u}(t,y,k) = \sum_{m\in\mathbb{N}} (\mathbb{P}_m \widetilde{u}) = \sum_{m\in\mathbb{N}} C_m(t,k)\varphi_m(y,k)\,, \tag{2.15}$$

and we likewise decompose $\widetilde{v}(t,y,k)$ as

$$\widetilde{v}(t,y,k) = \sum_{m\in\mathbb{N}} (\mathbb{P}_m \widetilde{v}) = \sum_{m\in\mathbb{N}} D_m(t,k)\varphi_m(y,k)\,. \tag{2.16}$$

Of course, in our numerical implementation, we have to truncate this summations at a certain fixed $M \in \mathbb{N}$. This M has to be chosen large enough to ensure mass conservation, i.e. conservation of the (discrete) L^2-norm. In the following we typically choose $M = 32$. By (2.3), this consequently yields the following evolutionary equation for the coefficients $C_m(t,k)$ and $D_m(t,k)$

$$\frac{\partial C_m}{\partial t} = D_m, \qquad \frac{\partial D_m}{\partial t} = -\frac{E_m^2(k)}{\varepsilon^2}\, C_m. \tag{2.17}$$

The corresponding solutions are given by

$$C_m(t,k) = \frac{1}{2}\left(C_m(0,k) - \frac{\mathrm{i}\varepsilon D_m(0,k)}{E_m(k)}\right)\mathrm{e}^{\mathrm{i}E_m(k)t/\varepsilon} + \frac{1}{2}\left(C_m(0,k) + \frac{\mathrm{i}\varepsilon D_m(0,k)}{E_m(k)}\right)\mathrm{e}^{-\mathrm{i}E_m(k)t/\varepsilon},$$

and similarly

$$D_m(t,k) = \frac{1}{2}\left(D_m(0,k) + \frac{\mathrm{i}E_m(k)C_m(0,k)}{\varepsilon}\right)\mathrm{e}^{\mathrm{i}E_m(k)t/\varepsilon} + \frac{1}{2}\left(D_m(0,k) - \frac{\mathrm{i}E_m(k)C_m(0,k)}{\varepsilon}\right)\mathrm{e}^{-\mathrm{i}E_m(k)t/\varepsilon}.$$

We consequently obtain $\widetilde{u}$ and $\widetilde{v}$ at the time $t^* = t + \triangle t$ by summing up all band contributions, i.e.

$$\widetilde{u}(t^*,y,k) = \sum_{m\in\mathbb{N}} C_m^\varepsilon(t^*,k)\varphi_m(y,k)\,, \quad \widetilde{v}(t^*,y,k) = \sum_{m\in\mathbb{N}} D_m^\varepsilon(t^*,k)\varphi_m(y,k)\,. \tag{2.18}$$

Finally, we perform the inverse transformation (2.12), to obtain

$$u(t^*,y) = \mathcal{T}^{-1}\widetilde{u}(t^*t,y,k), \quad v(t^*,y) = \mathcal{T}^{-1}\widetilde{v}(t^*,y,k), \tag{2.19}$$

which concludes the numerical procedure performed within Step 1.

Step 2. In the second step, we solve the ordinary differential equations

$$\frac{\partial u}{\partial t} = 0, \quad \frac{\partial v}{\partial t} = f(x), \tag{2.20}$$

on the same time-interval as before, where the solution obtained in Step 1 serves as initial condition for Step 2. Clearly, these equations can be solved exactly via

$$u(t,x) = u(0,x), \quad v(t,x) = v(0,x) + tf(x). \tag{2.21}$$

The above given algorithm is (formally) first order in time. To obtain a second order method we shall implement it using Strang's splitting, i.e. we perform Step 1 with time-step $\triangle t/2$, then Step 2 with $\triangle t$ and finally once again Step 1 with $\triangle t/2$.

3. Numerical simulations and comparison to other methods

In this section, we present some numerical simulations to show the efficiency of our new method. In our numerical tests we will always choose $a_\Gamma(y)$ as

$$a_\Gamma(y) = 2 + \cos(y). \tag{3.1}$$

Concerning $W_\Gamma(y)$, we either choose it to be smooth and given by

$$W_\Gamma(y) = 1 + \cos(y), \tag{3.2}$$

or discontinuous, where

$$W_\Gamma(y) = 1 - \sum_{\gamma\in\mathbb{Z}} \mathbf{1}_{x\in\left[\frac{\pi}{2}+2\pi\gamma,\frac{3\pi}{2}+2\pi\gamma\right]}. \tag{3.3}$$

The latter is known as the Kronig-Penney model.

3.1. Pseudo-Spectral and Finite Volume Methods.

To show the efficiency of our new method, we shall compare it with the more traditional pseudo-spectral method and a finite volume scheme. Indeed, Pseudo-spectral schemes already proved to be successful in similar circumstances, cf. [4, 15]. Let us briefly sketch how one proceeds there:

Step 1. In the first step we solve, as before, the system

$$\frac{\partial u}{\partial t} = v, \qquad \frac{\partial v}{\partial t} = \frac{\partial}{\partial x}\left(a_\Gamma\left(\frac{x}{\varepsilon}\right)\frac{\partial u}{\partial x}\right) - \frac{1}{\varepsilon^2}W_\Gamma\left(\frac{x}{\varepsilon}\right)u, \tag{3.4}$$

on a fixed time-interval $\triangle t$. In contrast to the above approach we shall now invoke the Fast Fourier Transform and solve

$$\frac{\partial \hat{u}}{\partial t} = \hat{v}, \qquad \frac{\partial \hat{v}}{\partial t} = \mathrm{i}\xi\left(a_\Gamma\left(\frac{\cdot}{\varepsilon}\right)(\mathrm{i}\xi\hat{u})^\vee\right)^\wedge - \frac{1}{\varepsilon^2}\left(W_\Gamma\left(\frac{\cdot}{\varepsilon}\right)u\right)^\wedge, \tag{3.5}$$

where "$\wedge$" and "$\vee$" denotes the FFT and the inverse FFT, respectively and $\xi \in \mathbb{R}$ is the Fourier-dual variable to x.

Step 2. The second step is then as described above in (2.20), (2.21).

Again, we shall implement this scheme by using Strang's splitting to obtain a method which is (formally) second order in time. Thus, both methods essential differ in their treatment of the spatially periodic operators. For our method, this treatment is basically exact (up to truncation errors) but it requires some pre-processing, namely the computation of the Bloch bands.

Since the finite volume method nowadays is already classic, we do not go into further details but only refer to the book [17]. In order to compare the different numerical algorithms we denote by $u^{\mathrm{FV}}(t,x)$ the solution gained from the standard second order finite volume method [17], $u^{\mathrm{SP}}(t,x)$ the solution gained from the standard pseudo-spectral method, whereas $u^{\mathrm{BD}}(t,x)$ denotes the solution obtained by our new method based on Bloch's decomposition. All methods will be compared to an "exact" solution $u(t,x)$, which is obtained using a very fine spatial grid and very small time step. The corresponding numerical error will be computed as

$$E^{BD/SP/FV}(t) = \frac{\left\| u(t,\cdot) - u^{\mathrm{BD/SP/FV}}(t,\cdot)\right\|_{L^2(\mathbb{R})}}{\|u(t,\cdot)\|_{L^2(\mathbb{R})}}.$$

3.2. **Numerical simulations.** We shall first consider two examples of linear Klein-Gordon waves in periodic media and then study a nonlinear case.

Example 3.1. (Linear waves without forcing) Consider the Klein-Gordon problem (1.2) with $f(x) \equiv 0$ and ε-independent initial data

$$u_0(x) = \left(\frac{2\nu}{\pi}\right)^{1/4} \mathrm{e}^{-\nu(x-\pi)^2}, \quad v_0(x) = 0. \tag{3.6}$$

In the following we will only show the case where $\nu = 6$.

Since in this case, we do not include a slowly varying forcing term $f(x)$, our Bloch-decomposition based method can solve the problem in one step, i.e $\triangle t = T$. But in order to have a fair comparison between the three methods, we note that for the finite-volume and the pseudo-spectral scheme we need to choose $\triangle t/\triangle x = \mathcal{O}(\varepsilon)$ according to their CFL condition. We therefore have to choose $\triangle t$ small enough in order to extract the corresponding convergence rates. Nevertheless, Table 2 shows that one still obtains quite poor convergence rates for SP and FV, if W_Γ is non-smooth. More precisely, Table 1 shows that our new method achieves spectral convergence in space even for a single time-step computation. In comparison to that the standard pseudo-spectral method and the finite volume scheme achieve spectral/second order convergence in space and second order convergence in time only for $\triangle t \ll \varepsilon$. From Table 2 we conclude that even if W_Γ is non-smooth, our new method still achieves spectral convergence with $\triangle t = T$. In this case, the other two methods are even worse, as they achieve only first order convergence in space. The advantage of our method becomes more apparent as ε becomes smaller.

TABLE 1. Convergence tests for Example 3.1 with a_Γ given by (3.1), W_Γ given by (3.2), $t = 0.1$, $\varepsilon = \frac{1}{32}$. For BD: $\triangle t = 0.1$, for SP and FV: $\triangle t = \frac{1}{100000}$.

$\triangle x$	$\pi/128$	$\pi/256$	$\pi/512$	$\pi/1024$
$E^{BD}(t)$	6.92E − 3	9.01E − 4	9.12E − 6	6.58E − 10
Convergence order		2.9	6.6	13.8
$E^{SP}(t)$	5.45E − 3	7.84E − 4	8.08E − 6	5.27E − 9
Convergence order		2.8	6.6	10.6
$E^{FV}(t)$	1.72E − 2	4.68E − 3	1.19E − 3	2.98E − 4
Convergence order		1.9	2.0	2.0

TABLE 2. Convergence tests for Example 3.1 with a_Γ given by (3.1), W_Γ given by (3.3), $t = 0.1$, $\varepsilon = \frac{1}{32}$. For BD: $\triangle t = 0.1$, for SP and FV: $\triangle t = \frac{1}{100000}$.

$\triangle x$	$\pi/128$	$\pi/256$	$\pi/512$	$\pi/1024$
$E^{BD}(t)$	5.17E − 3	7.16E − 4	6.65E − 5	1.09E − 6
Convergence order		2.8	3.4	5.9
$E^{SP}(t)$	1.16E − 1	5.54E − 2	2.70E − 2	1.33E − 2
Convergence order		1.1	1.0	1.0
$E^{FV}(t)$	1.24E − 1	5.75E − 2	2.76E − 2	1.35E − 2
Convergence order		1.1	1.0	1.0

Example 3.2. (Oscillatory initial data) Consider the Klein-Gordon equation (1.2) with a forcing term given by

$$f(x) = \left(\frac{2}{\pi\varepsilon^\beta}\right)^{1/4} \mathrm{e}^{-(x-\pi)^2}. \tag{3.7}$$

Here, $\beta > 0$ is some given parameter, describing the strength of the forcing. The case where $\beta = 2$ is the physically most relevant one but we shall also consider other cases, cf. Figure 1. The initial data are now assumed to be in *WKB-type form*, i.e. including ε-oscillations. More precisely we choose

$$u_0(x) = \alpha(x)\cos\left(\frac{kx}{\varepsilon}\right), \quad v_0(x) = \frac{\alpha(x)}{\varepsilon}\sin\left(\frac{kx}{\varepsilon}\right), \tag{3.8}$$

where the ε-independent amplitude $\alpha(x)$ is given by

$$\alpha(x) = \left(\frac{2\nu}{\pi}\right)^{1/4} \mathrm{e}^{-\nu(x-\pi)^2}. \tag{3.9}$$

In the following we will only show the results for $\nu = 6$ and $k = 1$. This WKB initial data describe spatially modulated waves with rapidly varying phase [5].

The results for this example are shown in Figure 1 and Tables 3–4: Because of the presence of a source term, we can no longer do a "one-step computation" as above. Nevertheless we can still use quite large time steps $\triangle t$, to get the satisfactory results. For smooth W_Γ, the Bloch-decomposition based method and the pseudo-spectral scheme yield spectral convergence rates in space and since we use Strang's splitting, the discretization errors in time are $\mathcal{O}(\triangle t^2)$. However, the Bloch-decomposition based method allows for much bigger time steps. In particular, we can choose time-steps which are *independent* of ε. Also note that even in cases where both methods have the same spatial and temporal convergence order, our new method yields a smaller error w.r.t. the exact solution.

For a non-smooth coefficient W_Γ, the Bloch-decomposition based method is still spectrally accurate in space and second order in time, while the pseudo-spectral scheme, roughly speaking, is only first order in space and at most first order in time.

TABLE 3. Convergence tests for Example 3.2 with a_Γ given by (3.1), W_Γ given by (3.2), $t = 0.1$, $\varepsilon = \frac{1}{128}$, and $\beta = 2$.

$\triangle t = \frac{1}{100000}$				
$\triangle x$	$\pi/256$	$\pi/512$	$\pi/1024$	$\pi/2048$
$E^{BD}(t)$	2.83E − 1	5.83E − 2	1.85E − 3	4.04E − 6
Convergence order		2.3	5.0	8.8
$E^{SP}(t)$	1.55E − 1	5.04E − 2	1.21E − 2	2.93E − 4
Convergence order		1.6	2.1	5.4
$\triangle x = \frac{\pi}{8192}$				
$\triangle t$	1/40	1/80	1/160	1/320
$E^{BD}(t)$	1.76E − 1	4.16E − 2	1.02E − 2	2.54E − 3
Convergence order		2.0	2.0	2.0
$\triangle t$	1/160	1/320	1/640	1/1280
$E^{SP}(t)$	4.53E − 1	1.13E − 1	2.83E − 2	7.05E − 3
Convergence order		2.0	2.0	2.0

TABLE 4. Convergence tests for Example 3.2 with a_Γ given by (3.1), W_Γ given by (3.3), $t = 0.1$, $\varepsilon = \frac{1}{128}$, and $\beta = 2$.

$\triangle t = \frac{1}{100000}$				
$\triangle x$	$\pi/256$	$\pi/512$	$\pi/1024$	$\pi/2048$
$E^{BD}(t)$	6.75E − 1	1.38E − 1	4.04E − 3	1.31E − 5
Convergence order		2.3	5.1	8.3
$E^{SP}(t)$	7.63E − 1	3.75E − 1	1.77E − 1	8.85E − 2
Convergence order		1.1	1.0	1.0
$\triangle x = \frac{\pi}{8192}$				
$\triangle t$	1/50	1/100	1/200	1/400
$E^{BD}(t)$	2.34E − 1	5.64E − 2	1.39E − 2	3.50E − 3
Convergence order		2.1	2.0	2.0
$\triangle t$	1/2000	1/4000	1/8000	1/16000
$E^{SP}(t)$	8.52E − 2	4.52E − 2	2.41E − 2	1.38E − 2
Convergence order		0.9	0.9	0.8

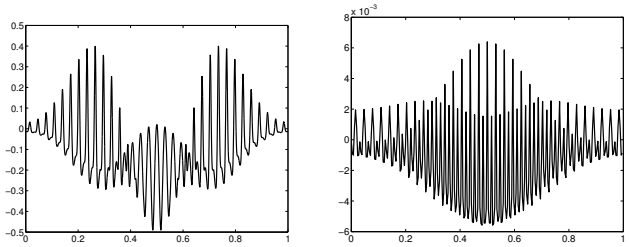

$u(1, 2\pi x)$ and $u(1, 2\pi x) - u^{\mathrm{BD}}(1, 2\pi x)$, $\beta = 0$.

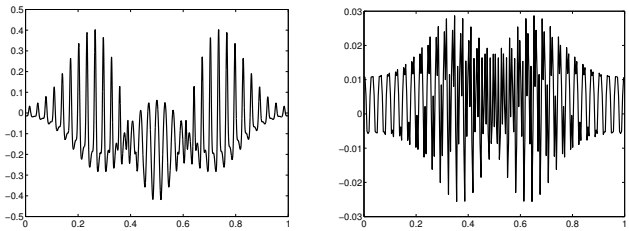

$u(1, 2\pi x)$ and $u(1, 2\pi x) - u^{\mathrm{BD}}(1, 2\pi x)$, $\beta = 1$.

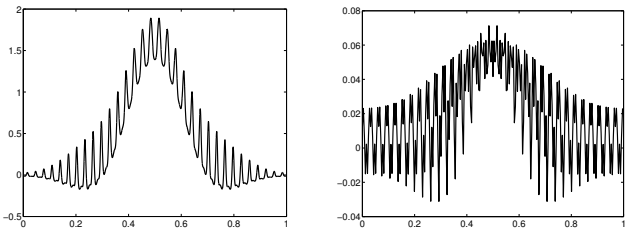

$u(1, 2\pi x)$ and $u(1, 2\pi x) - u^{\mathrm{BD}}(1, 2\pi x)$, $\beta = 2$.

FIGURE 1. Example 3.2: a_Γ given by (3.1), W_Γ given by (3.3), $\varepsilon = \frac{1}{32}$, $\triangle t = \frac{1}{10}$, $\triangle x = \frac{\pi}{512}$.

Finally we shall also consider a nonlinear version of (1.2), which is motivated by the model of light propagation in a Kerr medium (1.1).

Example 3.3. (Nonlinear wave propagation) Consider the following Klein-Gordon equation with cubic nonlinearity

$$\frac{\partial^2 u}{\partial t^2} = \frac{\partial}{\partial x}\left(a_\Gamma\left(\frac{x}{\varepsilon}\right)\frac{\partial u}{\partial x}\right) - \frac{1}{\varepsilon^2} W_\Gamma\left(\frac{x}{\varepsilon}\right) u + \varepsilon^{\kappa-2}\chi\left(\frac{x}{\varepsilon}\right) u^3. \tag{3.10}$$

where $\kappa > 0$, describes the strength of the nonlinearity. In the following we choose

$$\chi(y) = \cos(y) \tag{3.11}$$

to describe the nonlinear response of the periodic medium. Of particular interest in this setting is the problem of *nonlinear interaction* of Bloch bands. In [14] we did an extensive numerical study of this problem in the case of nonlinear Schrödinger equations. In order to study, at least qualitatively, this problem also for the class of equations given by (3.10) we shall in the following consider an initial data u_0, which is concentrated in a *single* Bloch band. More precisely we choose

$$u_0(x) = \mathbb{P}_{m_0}\left(\left(\frac{1}{\pi}\right)^{1/4} \mathrm{e}^{-\frac{(x-\pi)^2}{2\varepsilon}}\right), \quad v_0(x) = 0. \tag{3.12}$$

where $\mathbb{P}_{m_0}$ denotes the projection onto the m_0-th band as defined in (2.7). In the following we shall only show the results for $m_0 = 1$ and a non-smooth W_Γ given by (3.3).

Figure 2, shows the numerical results without nonlinear term. Note that in this case the m_0-th band is stable under the time-evolution, i.e. there is no energy-transfer to other bands. In Figure 3, the numerical results for different choices of κ are shown. We can see that when κ becomes smaller, there will more energy transfer between the bands, caused by the nonlinearity. Note that in the so-called *weakly nonlinear case* where $\kappa \geq 2$, our numerical results are consistent with those given in [24].

Finally we shall also in this nonlinear case compare our new numerical scheme to the traditional pseudo-spectral method. The results for $\kappa = 3$ are shown in Table 5. Our new method again yields better convergence rates than the traditional approaches.

TABLE 5. Convergence tests for example 3.3, $t = 1$, $\varepsilon = \frac{1}{32}$, $\kappa = 3$.

$\triangle t = \frac{1}{10000}$

$\triangle x$	$\pi/128$	$\pi/256$	$\pi/512$	$\pi/1024$
$E^{BD}(t)$	$4.51\mathrm{E}-1$	$6.03\mathrm{E}-2$	$2.86\mathrm{E}-3$	$2.99\mathrm{E}-6$
Convergence order		2.9	4.4	9.9
$E^{SP}(t)$	$6.51\mathrm{E}-1$	$3.35\mathrm{E}-1$	$1.87\mathrm{E}-1$	$1.01\mathrm{E}-1$
Convergence order		1.0	0.8	0.9

$\triangle x = \frac{\pi}{8192}$

$\triangle t$	1/10	1/20	1/40	1/80
$E^{BD}(t)$	$6.02\mathrm{E}-2$	$1.36\mathrm{E}-2$	$3.33\mathrm{E}-3$	$8.25\mathrm{E}-4$
Convergence order		2.1	2.0	2.0
$\triangle t$	1/100	1/200	1/400	1/800
$E^{SP}(t)$	$6.36\mathrm{E}-2$	$2.28\mathrm{E}-2$	$8.77\mathrm{E}-3$	$4.49\mathrm{E}-3$
Convergence order		1.5	1.4	1.0

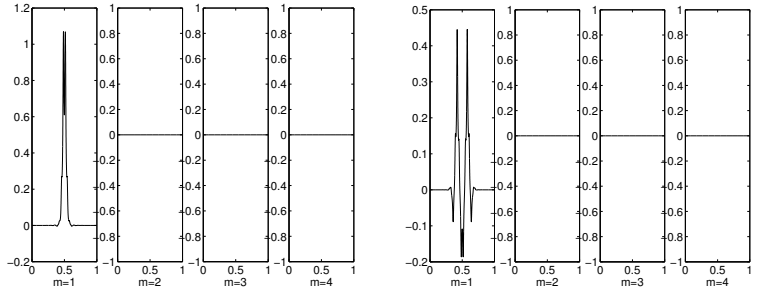

$\mathbb{P}_m u(0, 2\pi x)$ and $\mathbb{P}_m u(1, 2\pi x)$,.

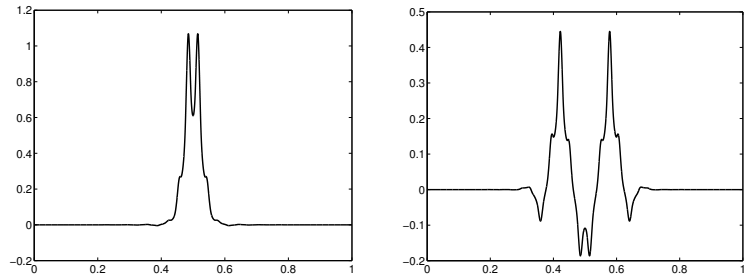

$u(0, 2\pi x)$ and $u(1, 2\pi x)$.

FIGURE 2. Example 3.3: $\chi \equiv 0$, $\varepsilon = \frac{1}{32}$, $\triangle t = \frac{1}{10}$, $\triangle x = \frac{\pi}{512}$.

In summary we find that in our method the time-steps can be chosen substantially larger than for the traditional pseudo-spectral method or the finite volume scheme. Indeed it is shown by the given examples, that our method (which moreover is unconditionally stable) is always spectrally accurate in space and second order in time even in a weakly nonlinear problem and even in situations with non-smooth coefficients.

4. Random coefficients: Stability tests and Anderson localization

In this last section we present numerical studies for the Klein-Gordon equation (1.2) including random coefficients. This describes waves propagating in *disordered media*, a topic of intense physical and mathematical research, cf. [21] for a general introduction. To this end, we shall first study the stability of our method w.r.t. to random perturbations.

4.1. **Stability of the Bloch-decomposition based algorithm.**

The purely periodic coefficients $a_\Gamma(y)$ and $W_\Gamma(y)$ describe an idealized situation where no defects are present within the material. More realistic descriptions for disordered media usually rely on the introduction of random perturbations within these coefficients and we wish to include such random perturbations also in our numerics. Since our numerical method relies on $\{\varphi_m(y,k)\}_{m=1}^M$ as basis functions, the stability of our method w.r.t. to perturbation of these Bloch functions is an important question.

To this end we consider, instead of (2.3), (2.4), the *randomly perturbed* eigenvalue problem

$$\left(-\frac{\partial}{\partial_y}\Big(a_\Gamma(\omega,y)\frac{\partial}{\partial_y}\Big) + W_\Gamma(y)\right)\varphi_m(\omega,y,k) = \lambda_m(\omega,k)\varphi_m(\omega,y,k), \tag{4.1}$$

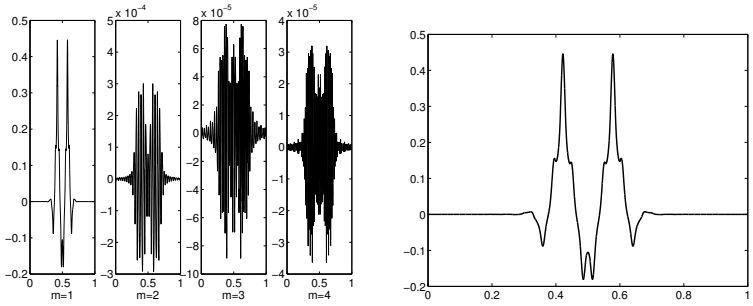

$\mathbb{P}_m u(1, 2\pi x)$ and $u(1, 2\pi x)$, $\kappa = 4$.

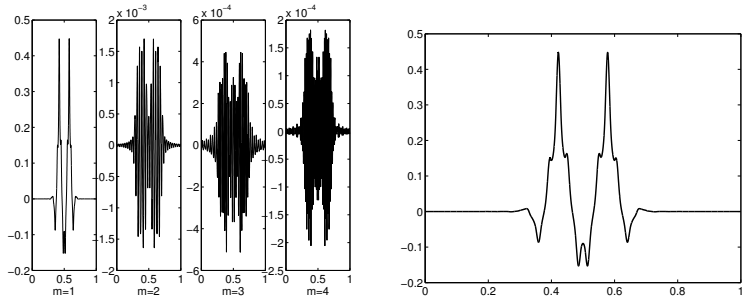

$\mathbb{P}_m u(1, 2\pi x)$ and $u(1, 2\pi x)$, $\kappa = 3.5$.

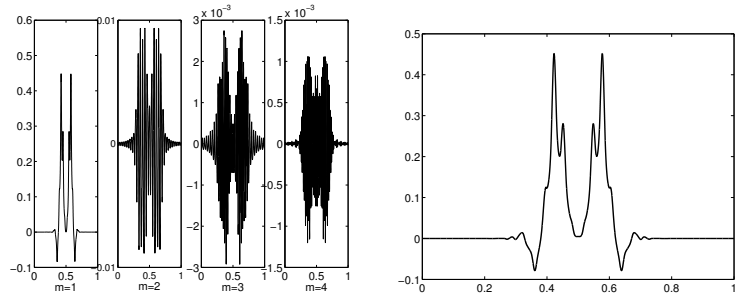

$\mathbb{P}_m u(1, 2\pi x)$ and $u(1, 2\pi x)$, $\kappa = 3$.

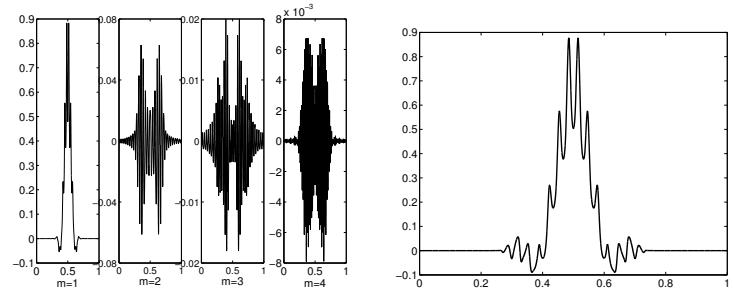

$\mathbb{P}_m u(1, 2\pi x)$ and $u(1, 2\pi x)$, $\kappa = 2.5$.

FIGURE 3. Example 3.3: Here $\varepsilon = \frac{1}{32}$, $\triangle t = \frac{1}{10}$, $\triangle x = \frac{\pi}{512}$.

subject to the quasi-periodic boundary condition. Here, the coefficient $a_\Gamma = a_\Gamma(\omega, y)$ is assumed to be a function of a uniformly distributed random variable ω with mean zero and variance $\sigma^2 \geq 0$. In the following we shall vary σ in such a way that we do not loose the uniform ellipticity, i.e. we have, as before, that

$\lambda_m(\omega,k) \geq 0$ (for every realization of ω) and we consequently set $E_m(\omega,k) = \sqrt{\lambda_m(\omega,k)}$. Note that we do *not* any assume randomness in W_Γ, since this would only result in a shift of the eigenvalues.

In our algorithm we shall now solve the random eigenvalue problem (4.1), for different choices of σ, to obtain the corresponding eigenvalues $\lambda_m(\omega,k)$ and eigenfunctions $\varphi_m(\omega,y,k)$. We shall then take the average of them and use these averaged quantities in our Bloch decomposition based algorithm (as described in Section 2). The solution of (1.2) which is obtained via this procedure will be denoted by $u^\sigma(t,x)$ and we shall compare it (for different choices of σ) to $u(t,x)$, which is the solution to the same equation without noise, i.e. where $a_\Gamma = a_\Gamma(y)$.

Example 4.1. (Stability test) Consider (1.2) with $f(x) \equiv 0$ and initial data

$$u_0(x) = \left(\frac{2}{\pi\varepsilon}\right)^{1/4} \mathrm{e}^{-\frac{(x-\pi)^2}{\varepsilon}}, \quad v_0(x) = 0. \tag{4.2}$$

The random coefficient a_Γ is chosen as

$$a_\Gamma(\omega,y) = a_\Gamma(y) + \omega, \quad a_\Gamma(y) = 2.5 + \cos(y), \tag{4.3}$$

i.e. including an *additive noise*. For a given choice of σ we numerically generate $N \in \mathbb{N}$ realizations of ω and consequently take the ensemble average. In our examples we usually choose $N = 100$. Figure 4 shows the average of the first few Bloch bands, i.e.

$$E_m(k) := \mathbb{E}\{E_m(\omega,k)\} \approx \frac{1}{N}\sum_{\ell=1}^{N} E_m(\omega_\ell,k), \tag{4.4}$$

for different values of σ.

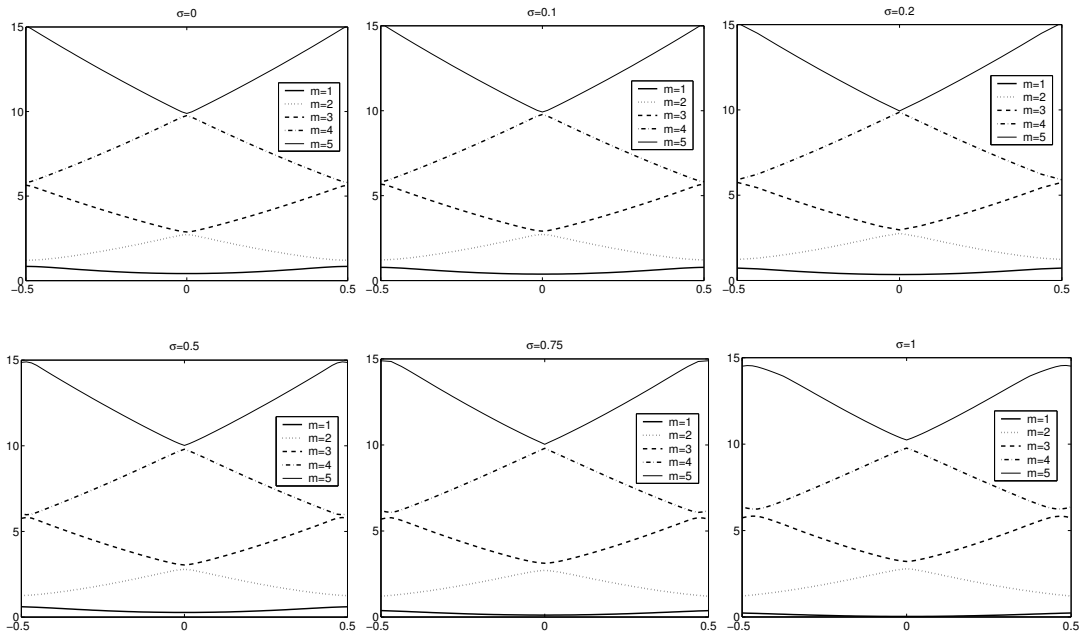

FIGURE 4. Example 4.1: The first five averaged Bloch bands $E_m(k) = \mathbb{E}\{E_m^\omega(k)\}$ for different choices of σ.

In Figure 5, we show a comparison between the solution $u^\sigma(t,x)$ with noise and the solution $u(t,x)$ without noise. To this end we consider two different kinds of errors

$$\Delta_\infty^\sigma(t) := \|u(t,\cdot) - u^\sigma(t,\cdot)\|_{L^\infty(\mathbb{R})}, \quad \Delta_2^\sigma(t) := \|u(t,\cdot) - u^\sigma(t,\cdot)\|_{L^2(\mathbb{R})}. \tag{4.5}$$

Numerically, we find that $\Delta_\infty^\sigma \sim \sigma$, and $\Delta_2^\sigma \sim \sigma\|u(t,\cdot)\|_{L^2(\mathbb{R})}$.

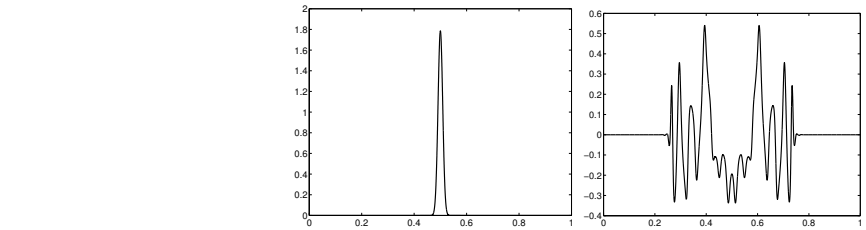

$u(0, 2\pi x)$ and $u(1, 2\pi x)$

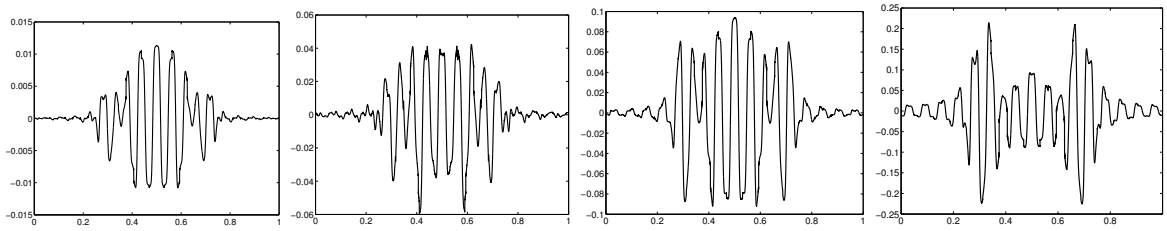

$u(1, 2\pi x) - u^\sigma(1, 2\pi x)$, for $\sigma = 0.01,\ 0.05,\ 0.1,\ 0.2$.

FIGURE 5. Example 4.1: $\varepsilon = \frac{1}{32}$, $\triangle t = \frac{1}{10}$, $\triangle x = \frac{\pi}{512}$.

We shall finally turn our attention to the numerical study of so-called *Anderson's localization*.

4.2. **Numerical Evidence for the Anderson's localization.** The phenomenon of Anderson's localization, also known as the *strong localization*, describes the absence of dispersion for waves in random media with sufficiently strong random perturbations. It has been predicted by P. W. Anderson in the context of (quantum mechanical) electron dynamics [2] but is now regarded as a general wave phenomenon that applies to the transport of electromagnetic or acoustic waves as well, cf. [7, 25, 27].

In the following, we shall again assume that $a_\Gamma = a_\Gamma(\omega, y)$ depends on a uniformly distributed random variable ω with mean zero and variance σ^2. We then study the random Klein-Gordon equation

$$\begin{cases} \dfrac{\partial^2 u^\omega}{\partial t^2} = \dfrac{\partial}{\partial x}\left(a_\Gamma\left(\omega, \dfrac{x}{\varepsilon}\right)\dfrac{\partial u^\omega}{\partial x}\right) - \dfrac{1}{\varepsilon^2} W_\Gamma\left(\dfrac{x}{\varepsilon}\right) u^\omega + f(x), \\ u^\omega\big|_{t=0} = u_0(x), \quad \dfrac{\partial u^\omega}{\partial t}\big|_{t=0} = v_0(x), \end{cases} \tag{4.6}$$

which describes the propagation of waves in disordered media. In order to realize the emergence of this localization phenomena we consider the *local energy density* $e^\omega(t,x)$ of the solution $u^\omega(t,x)$ given by [5]

$$e^\omega(t,x) := \frac{1}{2}\left(\left|\frac{\partial u^\omega}{\partial t}\right|^2 + a_\Gamma\left(\omega, \frac{x}{\varepsilon}\right)\left|\frac{\partial u^\omega}{\partial x}\right|^2 + \frac{1}{\varepsilon^2} W_\Gamma\left(\frac{x}{\varepsilon}\right)|u^\omega|^2\right). \tag{4.7}$$

The *total energy* $E_0^\omega(t)$ of $u^\omega(t,x)$ is then given by the zeroth spatial moment of $e^\omega(t,x)$, i.e.

$$E_0^\omega(\omega, t) = \int_{\mathbb{R}} e^\omega(t,x)\mathrm{d}x, \tag{4.8}$$

and we likewise define

$$E_2^\omega(\omega,t)=\int_{\mathbb{R}} x^2 e^\omega(t,x)\mathrm{d}x, \tag{4.9}$$

which measures the spread of the wave. It represents the mean square of the distance of the wave from the origin at time t. Note that in the case, where $f(x)\equiv 0$ (no source term), we have energy conservation, i.e. $E_0^\omega(t)=E_0^\omega(0)$. We consequently consider the function

$$A(t):=\frac{\mathbb{E}\{E_2^\omega(t)\}}{\mathbb{E}\{E_0^\omega(t)\}}, \tag{4.10}$$

where $\mathbb{E}$ again denotes the mathematical expectation. The quantity $A(t)$ has been introduced in [9] as a measure for the presence of Anderson's localization. In the absence of any random perturbation $A(t)$ should grow quadratically in time whereas in the case of the Anderson localization $A(t)$ should grow only linearly (indicating diffusive behavior) and eventually become a constant in time [9, 25, 27].

Example 4.2. (Anderson's localization for additive noise) Here we also consider (4.6) with $f(x)\equiv 0$ and $a_\Gamma(\omega,y)$ is given by (4.3), the potential W_Γ is given by (3.3) and the initial data are chosen as (4.2). Now we do a different test with random perturbation. We then solve the Klein-Gordon equation (4.6) with 100 different realizations of the random variable ω. Finally we take an ensemble average to obtain $\mathbb{E}\{u^\omega(t,x)\}$, cf. Figure 6.

Figure 7 shows the behavior of the function $A(t)$: As we see it first grows almost linearly in t, a typical diffusive behavior, and then, around $t=2$ it flattens. The latter is a strong indication of Anderson's localization [2, 7, 9, 25, 27].

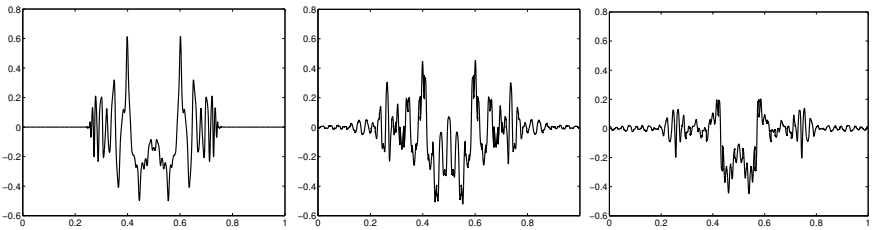

$\mathbb{E}\{u^\omega(1,1\pi x)\}$, where, from left to right: $\sigma=0$, 0.5, and 1.0.

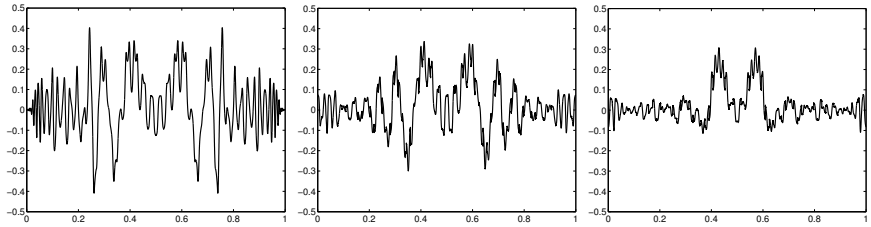

$\mathbb{E}\{u^\omega(2,1\pi x)\}$, where, from left to right: $\sigma=0$, 0.5, and 1.0.

FIGURE 6. Example 4.2: The averaged solution at time $t=1$ and $t=2$ for different choices of σ ($\varepsilon=\frac{1}{64}$).

Example 4.3. (Anderson's localization for multiplicative noise) Finally, consider (4.6) with $f(x)\equiv 0$, W_Γ given by (3.3), and the same initial data as before, but this time we choose

$$a_\Gamma(\omega,y)=1.5+\omega\, a_\Gamma(y),\quad a_\Gamma(y)=\cos(y), \tag{4.11}$$

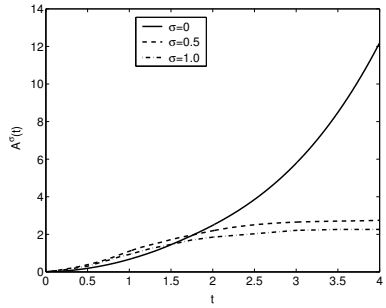

FIGURE 7. Example 4.2: The graphs of $A(t)$ for different σ ($\varepsilon = \frac{1}{64}$).

i.e. a multiplicative noise. The initial data u_0, v_0 and the coefficient W_Γ are chosen as in Example 4.2 above. The results shown in Figure 8 are qualitatively similar to those found before. Thus we again have numerical evidence for the emergence of Anderson's localization.

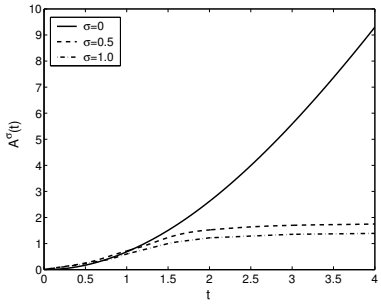

FIGURE 8. Example 4.3: the graphs of $A(t)$ for different choices of σ ($\varepsilon = \frac{1}{64}$).

REFERENCES

1. G. Allaire, *Dispersive limits in the homogenization of the wave equation*, Annales de la Facult'e des Sciences de Toulouse XII (2003), 415–431.
2. P. W. Anderson, *The question of classical localization. A theory of white paint?* Philos. Mag. B, **52** (1985), 505–509.
3. N. W. Ashcroft and N. D. Mermin, *Solid state physics*, Saunders New York, 1976.
4. W. Z. Bao, S. Jin, and P. Markowich, *On time-splitting spectral approximations for the Schrödinger equation in the semiclassical regime*, J. Comp. Phys. **175** (2002), 487–524.
5. A. Bensoussan, J. L. Lions, and G. Papanicolaou, *Asymptotic Analysis for Periodic Structures*, North-Holland Pub. Co., 1978.
6. K. Busch, G. Schneider, L. Tkeshelashvili, and H. Uecker, *Justification of nonlinear Schrödinger equation in spatially periodic media*, Z. angew. Math. Phys. **57** (2006), 905–939.
7. C. A. Condat and T. R. Kirkpatrick, *Resonant scattering and Anderson localization of acoustic waves*, Phys. Rev. B, **36** (1987), 6782–6793.
8. T. R. Fogarty and R. J. LeVeque, *High-resolution finite-volume methods for acoustic waves in periodic and random media*, J. Acoust. Soc. Am. **106** (1999), 17–28.
9. J. Fröhlich and T. Spencer, *A Rigorous Approach to Anderson Localization*, Physics Reports, **103** (1984), 9–25.
10. P. Gérard, P. Markowich, N. Mauser, and F. Poupaud, *Homogenization Limits and Wigner transforms*, Comm. Pure and Appl. Math. **50** (1997), 323–378.

11. L. Gosse, *The numerical spectrum of a one-dimensional Schrödinger operator with two competing periodic potentials*, Commun. Math. Sci. **5** (2007), 485–493.
12. L. Gosse and P. A. Markowich, *Multiphase semiclassical approximation of an electron in a one-dimensional crystalline lattice - I. Homogeneous problems*, J. Comput Phys. **197** (2004), 387–417.
13. Z. Huang, S. Jin, P. Markowich, and C. Sparber, *A Bloch decomposition based split-step pseudo spectral method for quantum dynamics with periodic potentials*, SIAM J. Sci. Comput. **29** (2007), 515–538.
14. Z. Huang, S. Jin, P. Markowich, and C. Sparber, *Numerical simulation of the nonlinear Schrodinger equation with multi-dimensional periodic potentials*, Multiscale Model. Simul., (to appear)
15. Z. Huang, S. Jin, P. Markowich, C. Sparber and C. Zheng, *A Time-splitting spectral scheme for the Maxwell-Dirac system*, J. Comput. Phys. **208** (2005), 761–789.
16. J. Kevorkian and D. L. Bosley, *Multiple-scale homogenization for weakly nonlinear conservation laws with rapid spatial fluctuations*, Stud. Appl. Math. **101** (1998), 127–183.
17. R. J. LeVeque, *Finite Volume Methods for Hyperbolic Problems*, Cambridge University press, Cambridge, 2002.
18. P. A. Markowich, N. Mauser, and F. Poupaud, *A Wigner-function approach to (semi)classical limits: electrons in a periodic potential*, J. Math. Phys. **35** (1994), 1066–1094.
19. D. J. Mead, *Wave Propagation in Continuous Periodic Structures: Research Contributions from Southampton, 1964–1995*, Journal of Sound and Vibration, **190** (1996), 495–524.
20. M. Reed and B. Simon, *Methods of modern mathematical physics IV. Analysis of operators*, Academic Press, 1978.
21. P. A. Robinson, *Wave propagation in disordered media*, Phil. Magazine B **80** (2000), 2087–2108.
22. F. Santosa and W. W. Symes, *A Dispersive Effective Medium for Wave Propagation in Periodic Composites*, SIAM J. Appl. Math. **51** (1991), 984–1005.
23. E. Sanchez-Palencia, *Non-homogeneous Media and Vibration Theory*, Springer-Verlag, New York, 1980.
24. G. Schneider and H. Uecker, *The mathematics of light pulses in dispersive media*, DMV-Mitteilungen, to appear.
25. C. M. Soukoulis, E . N. Economou, G . S. Grest, and M. H. Cohen, *Existence of Anderson Localization of Classical Waves in a Random Two-Component Medium*, Phys. Rev. Lett. **62** (1989), 575–578.
26. S. Teufel, *Adiabatic perturbation theory in quantum dynamics*, Lecture Notes in Mathematics 1821, Springer, 2003.
27. R.L. Weaver, *Anderson localization in the time domain: Numerical sdudies of waves in two-dimensional disordered media*, Phys. Rev. B, **49** (1994), 5881–5895.
28. C. H. Wilcox, *Theory of Bloch waves*, J. d'Anal. Math. **33** (1978), 146–167.

(Z. Huang) Dept. of Mathematical Sciences, Tsinghua University, Beijing 100084, China

E-mail address: zhuang@math.tsinghua.edu.cn

(S. Jin) Dept. of Mathematics, University of Wisconsin, Madison, WI 53706, USA

E-mail address: jin@math.wisc.edu

(P. A. Markowich) Department of Applied Mathematics and Theoretical Physics, University of Cambridge, Wilberforce Road, Cambridge CB3 0WA & Faculty of Mathematics, University of Vienna, Nordbergstrasse 15, A-1090 Vienna, Austria

E-mail address: peter.markowich@univie.ac.at

(C. Sparber) Department of Applied Mathematics and Theoretical Physics, University of Cambridge, Wilberforce Road, Cambridge CB3 0WA

E-mail address: c.sparber@damtp.cam.ac.uk